COMMUNICATIONS PHYSICS

ARTICLE

DOI: 10.1038/s42005-017-0001-4 OPEN

Exotic multifractal conductance fluctuations in graphene

Kazi Rafsanjani Amin[1], Samriddhi Sankar Ray[2], Nairita Pal[1], Rahul Pandit[1] & Aveek Bid[1]

In quantum systems, signatures of multifractality are rare. They have been found only in the multiscaling of eigenfunctions at critical points. Here we demonstrate multifractality in the magnetic field-induced universal conductance fluctuations of the conductance in a quantum condensed matter system, namely, high-mobility single-layer graphene field-effect transistors. This multifractality decreases as the temperature increases or as doping moves the system away from the Dirac point. Our measurements and analysis present evidence for an incipient Anderson-localization near the Dirac point as the most plausible cause for this multifractality. Our experiments suggest that multifractality in the scaling behavior of local eigenfunctions are reflected in macroscopic transport coefficients. We conjecture that an incipient Anderson-localization transition may be the origin of this multifractality. It is possible that multifractality is ubiquitous in transport properties of low-dimensional systems. Indeed, our work suggests that we should look for multifractality in transport in other low-dimensional quantum condensed-matter systems.

[1] Department of Physics, Indian Institute of Science, Bangalore, Karnataka 560012, India. [2] International Centre for Theoretical Studies, Tata Institute of Fundamental Research, Bangalore, Karnataka 560089, India. Correspondence and requests for materials should be addressed to A.B. (email: aveek@iisc.ac.in)

One of the unsolved problems in single-layer graphene (SLG) is the nature of the electronic wave-function near the charge-neutrality (Dirac) point. In principle, the charge carrier density of SLG should be continuously tunable, down to zero, leading to the largely unexplored regime of extremely weak interactions in a low carrier density system. The interaction parameter r_s, which parametrizes the ratio of the average inter-electron Coulomb interaction energy to the Fermi energy, turns out to be independent of charge carrier density in the case of SLG where $r_s = e^2/(\kappa\hbar v_F)$. Here, κ is the dielectric constant of the surrounding medium and v_F is the Fermi velocity. In the case of SLG on an SiO_2 substrate, $r_s = 0.8$. Thus SLG is a very weakly interacting system, when compared to other conventional two-dimensional systems such as GaAs/AlGaAs and Si inversion layers, where the values of r_s are typically much higher. A naïve application of the scaling theory to such a system in this regime would predict Anderson localization—a disorder-driven quantum phase transition, leading to a complete localization of the charge carriers, and thence, to an insulator[1–5]. Indeed, theoretical calculations for graphene indicate that intervalley scattering can lead to changes in the local and averaged electronic density of states with the creation of localized states[6,7]. For example, graphene-terminated SiC (0001) surfaces undergo an Anderson localization transition upon dosing with small amounts of atomic hydrogen[8]. This intervalley scattering-induced localization is most effective near the Dirac point, where the screening of the impurity scatterers is negligible[7]. Experiments, however, find the appearance of a minimum conductance value at the Dirac point with $\sigma_{min} \approx 2e^2/\pi\hbar$, instead of a diverging resistance which is the hallmark of a truly localized state; notable exceptions being carrier localization[9] and an Anderson localization transition in bilayer graphene heterostructures[10].

By studying the scaling behavior of the universal conductance fluctuations (UCF), we look for signs of charge carrier localization near the Dirac point in ultra-high-mobility SLG and uncover, as a result, an exotic multifractal behavior in the UCF. Multifractality, characterized by an infinite number of scaling exponents, is ubiquitous in classical systems. Since the pioneering work of Mandelbrot[11], the detection and analysis of multifractal scaling in such systems have enhanced our understanding of several complex phenomena, e.g., the dynamics of the human heart beat[12], the form of critical wave-functions at the Anderson localization transition[1], the time series of the Sun's magnetic field[13], in medical signal analysis (for instance, in pattern recognition, texture analysis and segmentation)[14], fully developed turbulence and in a variety of chaotic systems[15,16]. In condensed matter systems, signatures of multifractality are usually sought in the scaling of eigenfunctions at critical points[17–24]. Despite compelling theoretical predictions[25–30], there are no reports of the successful observation of multifractality in transport coefficients.

Simple fractal conductance fluctuations, on the other hand, have been observed in several condensed matter systems[31–35]. These arise through semi-classical electron wave interference processes whenever a system has mixed chaotic regular dynamics[31,34,36,37]. In all these systems, a primary prerequisite for the observation of fractal transport is that the electron dynamics be amenable to semi-classical analysis—the fractal nature of conductance fluctuations seen in these systems disappears as the system is driven deep into the quantum limit. For such a mixed-phase semi-classical system, the graph of conductance (G) versus an externally applied magnetic field (B) has the same statistical properties as a Gaussian random process with increments of mean zero and variance $(\Delta B)^\gamma$. These processes are known as fractional Brownian motion and have the property that their graph is a fractal of dimension $D_F = 2 - \frac{\gamma}{2}$[31,34], with $1 \le D_F \le 2$.

A semi-classical description, however, breaks down in the case of materials where the charge carriers obey a Dirac dispersion relation, e.g., in graphene and topological insulators. In this report, we ask: can we find signatures of multifractality in a quantum system through transport measurements, specifically through the statistical properties of the graph of conductance fluctuations versus an external parameter like the magnetic field? We address this question by studying in detail the statistics of conductance fluctuations in high-mobility SLG–FET devices as a function of the perpendicular magnetic field over a wide range of temperature and doping levels. We report, for the first time, the occurrence of multifractality in the UCF in high-mobility graphene devices deep in the quantum limit. Our measurements and analysis suggest at an incipient Anderson localization transition in graphene near the Dirac point.

Results

Measurement of UCF. SLG–FET devices with mobilities in the range 20,000–30,000 $cm^2\,V^{-1}\,s^{-1}$ were fabricated on SiO_2 substrates by mechanical exfoliation from natural graphite, followed by conventional, electron-beam lithography[38] (Fig. 1a, b). We begin with the dependence of the resistance (R) on the gate voltage (V_G), for the device G28M6. In Fig. 1c we show plots of R versus $\Delta V_G = V_G - V_D$, where V_D is the Dirac point, measured at different temperatures (T). The high mobility and the position of the charge neutrality point very close to $V_G = 0$ V attests to the high quality of the devices. We measured the magnetoconductance (G) as a function of the magnetic field ($\boldsymbol{B} = (0, 0, B)$), applied perpendicular to the plane of the device, in the range $-0.2\ \mathrm{T} \le B \le 0.2\ \mathrm{T}$. The presence of UCF was confirmed by the appearance of reproducible, non-periodic, but magnetic-field-symmetric, oscillations in G. The measurements were performed on multiple devices, over a wide range of V_G and T. We find our UCF data to be in excellent agreement with previous studies of magnetoresistance and conductance fluctuations in SLG[39–43]. Figure 2a shows illustrative plots of $G(B)$ with the Fermi energy (E_F) maintained very close to the Dirac point ($\Delta V_G \simeq 0$) for the device G28M6. The data for other devices are similar and are shown in the Supplementary Figure 1 (see Supplementary Note 1). At low values of $|B|$, near the minimum of G at $B = 0$, weak-localization corrections are visible (Fig. 2a). As we move away from $B = 0$, the conductance fluctuations become prominent. The amplitudes of the UCF peaks, and the values of the charge carrier phase coherence length L_ϕ, obtained from the variance of the UCF (Fig. 2b), decrease with increasing temperature because of thermal dephasing (see Supplementary Note 2, Supplementary Figures 2, 3 and Supplementary Table 1 for a discussion on methods to obtain L_ϕ). The temperature dependence of the intervalley scattering length and the intravalley scattering length, extracted from weak localization measurements at $T = 20$ mK and $\Delta V_G = 0.2$ V, are shown in the Supplementary Figure 4 (see Supplementary Note 3). We find them to be in excellent agreement with previous studies of localization in SLG[42,44]. We also observe an increase in L_ϕ with increasing $|\Delta V_G| = |V_G - V_D|$ (Fig. 2c), which we attribute to the increase in the screening of impurities by charge carriers[39]. We note an apparent saturation of L_ϕ below a temperature of $\simeq 100$ mK. The saturation of the phase-coherence length (L_ϕ) with decreasing temperature is an issue that has been at the forefront of research in several other semiconducting materials including doped Si[45–47]. There are many effects, e.g., the presence of magnetic impurities[47] or finite size, which can lead to a saturation of L_ϕ. We note here that a decoupling of the electron and lattice temperature leading to a saturation of the L_ϕ is also possible. However, the data shown in Figs. 1c and 2a show a continuous

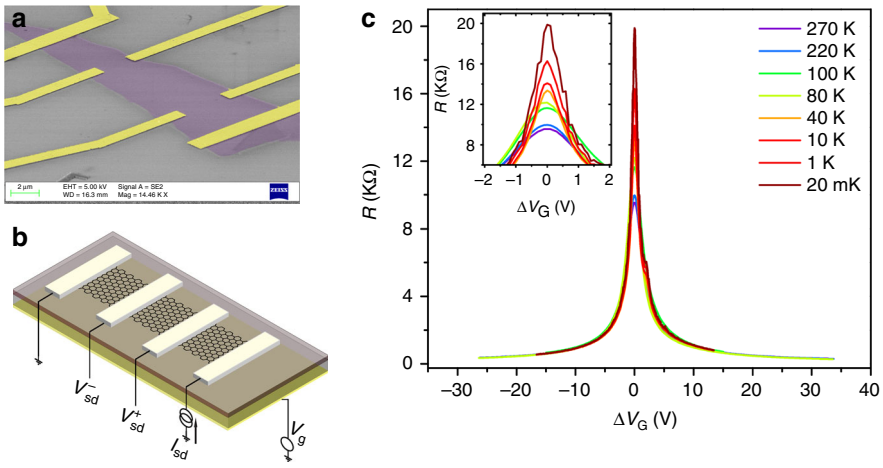

Fig. 1 Device structure and characteristics. **a** False-colour SEM image and **b** schematic device configuration of our SLG-FET. The scale-bar in **a** is 2 μm. **c** Plot of R versus ΔV_G, measured at different temperatures. The values of the temperatures at which the data were collected are mentioned in the legend. In the inset, we plot the same data, zoomed in near the Dirac point ($|\Delta V_G| \leq 2$ V)

evolution of both the conductance and conductance fluctuations down to 20 mK. This rules out any saturation of the electron temperature down to 20 mK, and hence, the observed saturation of L_ϕ below a certain temperature is not an experimental artifact (see Supplementary Note 3). In a separate set of measurements, we obtain the magnitude of the UCF, at a given magnetic field, by sweeping over V_G and calculating the rms value of the fluctuations. We found that this quantity decreased sharply with increasing magnetic field (see Supplementary Note 4, Supplementary Figure 5) in conformity with theoretical predictions[48].

Analysis of fractal scaling of the UCF. UCF represents quantum correction to Drude conductivity arising from the interference of electronic wavefunctions; it is a fingerprint of the disorder configuration in the conducting channel. Besides information about the phase-coherence of the charge carriers, it can also provide crucial insights into the electron dynamics and distribution of eigenstates through a scaling-dimension analysis of the magnetoconductance traces[31,32,34]. We first compute the simple fractal dimensions D_F of the UCF curves via the Ketzmerick variance method (see Supplementary Note 5, and Supplementary Figure 6 for details). Figure 3a shows plots of D_F versus T for the device G28M6. At very low T and small $|\Delta V_G|$, we find $1 < D_F < 2$. With increasing temperature, $D_F \to 1$ monotonically. In this high-T regime, the thermal-diffusion length $L_T = \sqrt{\hbar D/k_B T} \ll L_\phi$, with D the thermal diffusion coefficient of the charge carriers; therefore, quasiparticle phase decoherence, induced by inelastic thermal scattering, suppresses quantum interference. For large $|\Delta V_G|$, the magnitude of the UCF is comparable to, or smaller than the background electrical noise, so $D_F \to 2$, the value for Gaussian white noise. In Fig. 3b, we plot D_F versus L_ϕ for two different devices: G28M6 and G30M4; remarkably, all the data points from these two devices cluster in the vicinity of a curve, with $D_F \propto \ln(L_\phi)$. In the limits $L_\phi \ll L$, the UCF is non-fractal ($D_F \simeq 1$), whereas for large L_ϕ, the UCF is a fractal, so $1 < D_F < 2$.

Analysis of multifractal scaling of the UCF. We build upon the predictions of multifractal scaling of conductance fluctuations in quantum systems[25] by carrying out a multifractal detrended fluctuation analysis of our UCF (see Supplementary Note 6, Supplementary Figures 7 and 8 for details). The multifractality can be represented in the following two ways: (1) by the generalized Hurst exponent $h(q)$, defined using the order-q moment of the UCF as $\langle \mathrm{rms}[\Delta G(\Delta B)]^q \rangle^{1/q} \sim [\Delta B]^{h(q)}$, and (2) by the multifractal spectrum $f(\alpha)$, obtained from the Legendre transform of $h(q)$. For a monofractal function, $h(q)$ has a single, q-independent value. For each one of our UCF plots, we obtain $h(q)$ in the range $-4 \leq q \leq 4$. An illustrative plot of $h(q)$ versus q that we obtain from our magnetoconductance data at 20 mK (Fig. 4a) is shown in Fig. 4b; $h(q)$ goes smoothly from $\simeq 1.9$, at $q = -4$, to $\simeq 0.85$, at $q = 4$; the corresponding $f(\alpha)$ spectrum is plotted in Fig. 4c. The singularity spectra have a definite maximum value of 1 (which is the dimension of the support graph). The width of the multifractal spectrum is defined as $\Delta\alpha \equiv h(q)_{\max} - h(q)_{\min}$. The wide range of $h(q)$, or, equivalently, the wide spectrum ($\Delta\alpha = 1.05$) quantifies the multifractality of the UCF. This is the first observation of multifractality of a conductance in any quantum-condensed matter system and is the central result of our work.

We note that there are two distinct properties of UCF that can give rise to its multifractal behavior[49,50]: (i) a fat-tailed, non-Gaussian distribution of the UCF differences (as a function of δB) or (ii) long-range, in the magnetic field B, correlations of the fluctuations of $\delta g(B)$. We have verified that the distribution of our measured $\delta g(B)$ is not log-normal. Having ruled out (i), we now give a convenient test for (ii): we check for multifractality in a data set obtained from a random shuffling (see Supplementary Note 7) of the original sequence of $\delta g(B)$. If the long-range correlations (ii) exist, then signatures of multifractality must be absent in the reshuffled data. Indeed, in our experimental data, we observe a near-complete suppression of multifractality in the shuffled data set with $h_{\mathrm{shuf}}(q) \simeq 0.5$ for all values of q and $\Delta\alpha = 0.05$ (Supplementary Figure 9). Hence it is reasonable to infer that the multifractality in our UCF can be traced back to long-ranged correlations, that are otherwise difficult to measure.

Figure 4d shows plots of $f(\alpha)$ for different values of T and $\Delta V_G = 0.2$ V. The symmetry of $f(\alpha)$ about α_0 (Fig. 4c) reflects the distribution of fluctuations, about the mean of the UCF. The large-fluctuation (small-fluctuation) segments contribute predominantly to the $q > 0$ ($q < 0$) part of $h(q)$. The $q > 0$ ($q < 0$) part of $h(q)$ maps onto the $\alpha < \alpha_0$ ($\alpha > \alpha_0$) region of $f(\alpha)$, which is more-or-less symmetric about α_0 at low T (Fig. 4d). As we increase T, this symmetry is lost. The magnitude of the skewness $\langle [\delta\alpha]^3 \rangle / \langle [\delta\alpha]^2 \rangle^{3/2}$, where $\delta\alpha = (\alpha - \alpha_0)$, increases with T. Therefore, as T increases, large-amplitude conductance fluctuations become rarer than small-amplitude fluctuations. This is consistent with our plots of the UCF (Fig. 2a).

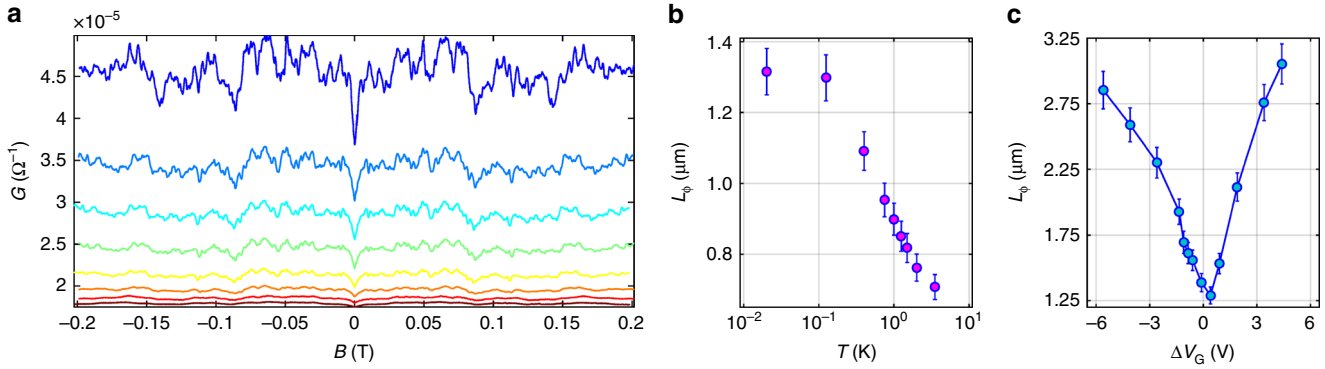

Fig. 2 UCF in graphene. **a** Illustrative plots of the magnetoconductance G versus the magnetic field B measured at 0.02, 0.05, 0.075, 0.10, 0.20, 0.50, 1.00, and 2.00 K (from top to bottom—curves for different temperatures have been shifted vertically for clarity). The data shown here are from the device G28M6 measured close to the Dirac point ($\Delta V_G = 0.2$ V). **b** Plot of the phase-coherence length L_ϕ versus the temperature T extracted from the UCF measured at $\Delta V_G = 0.2$ V. **c** Plot of L_ϕ versus ΔV_G, extracted from the UCF measured at $T = 20$ mK. The error-bars in **b**, **c** represent the standard deviation in L_ϕ

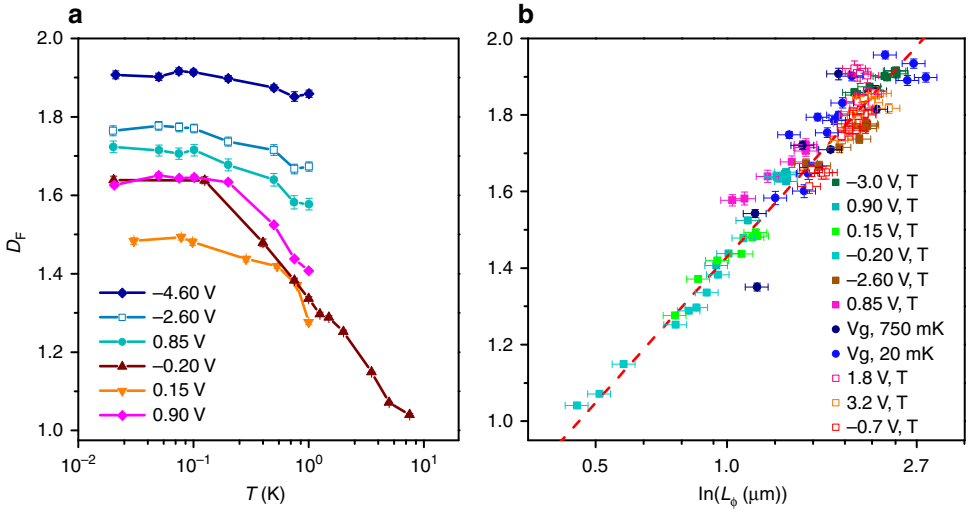

Fig. 3 Fractal dimension of UCF in graphene. **a** Plots of the fractal dimension D_F versus the temperature T for different values of ΔV_G. The error-bars represent the standard deviation in D_F. **b** D_F versus the charge carrier phase coherence length L_ϕ on a semi-log scale; the data points, with error bars representing standard deviation in D_F and L_ϕ, are from two different devices (filled symbols: G28M6; open symbols: G30M4) and for the following parameter ranges: 20 mK < T < 10 K and −4.5 V < ΔV_G < 4.5 V. The numbers in the legend refer to the (V_G, T) parameter space. The red curve is $D_F \propto \ln(L_\phi)$ (see text)

Discussion

A naïve characterization of the fractal property of a curve, say by the measurement of one fractal dimension, does not rule out multifractality of this curve, which requires the calculation of an infinite number of dimensions[51] (related to $h(q)$). One dimension suffices for monofractal scaling (as, e.g., in the scaling of velocity structure functions in the inverse cascade region of forced, two-dimensional fluid turbulence[52,53]). Our measurements of the UCF in SLG show that it is multifractal only if (i) the temperature is low and (ii) $\Delta V_G \simeq 0$. If either one of these conditions is not met, the plot of δg versus B is a monofractal (see Supplementary Note 8, and Supplementary Figure 10); at sufficiently large T, $D_F \to 1$ and the plots are non-fractal.

What can be the possible origin of our multifractal UCF? We list three potential causes: (1) scarring of wave functions (e.g., because of classically-chaotic billiards[54]); (2) quasi-periodicity in the Hamiltonian induced by a magnetic field[55–57] and its analog for graphene[58]; (3) Anderson localization-induced multi-fractality[1]. We critically examine each one of these possibilities below and conclude that our results are most compatible with the last of these mechanisms.

While describing a quantum system, whose classical analog is chaotic, one encounters scarred wavefunctions, whose intensity is enhanced along unstable, periodic orbits of the classical system. This non-uniform distribution of intensity of wavefunctions results from quasiparticle interference. Quantum scars can lead to pointer states[59] with long trapping times, and, consequently, to large conductance fluctuations. Relativistic quantum scars have been predicted theoretically in geometrically confined graphene stadia, which exhibit classical chaos[60]. However, our devices are not shaped like billiards that are classically chaotic; and the charge carriers are not in the ballistic regime. Therefore, quantum scars cannot be the underlying cause for our multifractal UCF.

Fractal energy spectra can arise in tight-binding problems with an external magnetic field, which can be mapped onto Schrödinger problems with quasiperiodic potentials[55–57,61]. It has been argued[58], therefore, that a fractal conductance can also arise, via Hofstadter-butterfly-type spectra, in Dirac systems at sufficiently

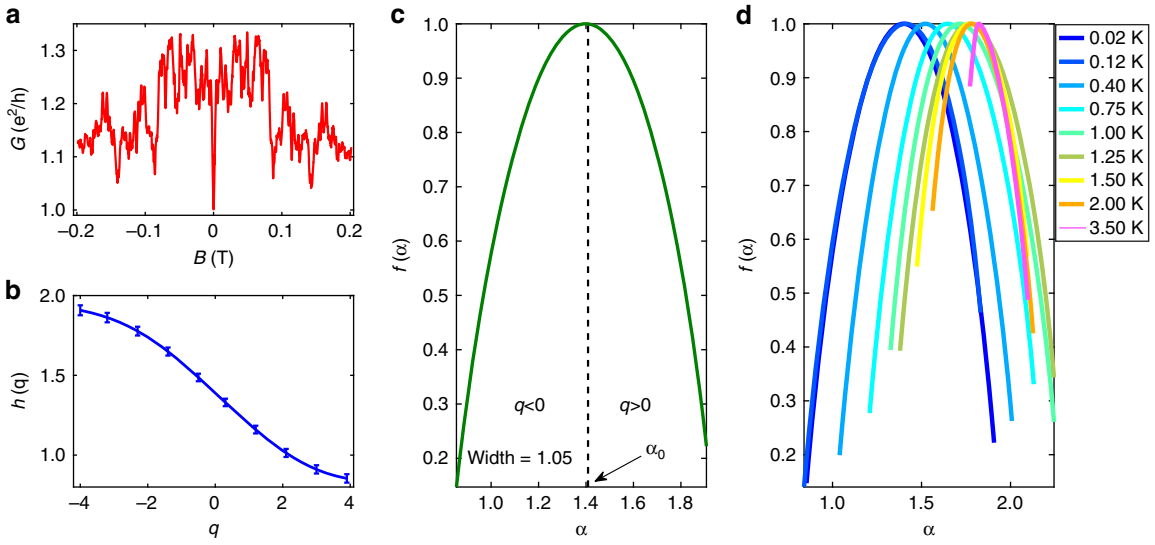

Fig. 4 Multifractality of UCF in graphene. **a** A typical plot of the magnetoconductance at $T = 20$ mK, $\Delta V_G = 0.2$ V for our device G28M6. **b** Plot of the generalized Hurst exponent $h(q)$ versus q, calculated from the UCF data in **a**. A few representative error bars, defining the standard deviation in the data, are shown in the plot. **c** Plot of the multifractal singularity spectrum $f(\alpha)$ versus α that follows from the $h(q)$ versus q data plotted in **b**. The dotted vertical line marks the location of the maximum of $f(\alpha)$. **d** Plots illustrating the temperature dependence of $f(\alpha)$ at $\Delta V_G = 0.2$ V for the device G28M6

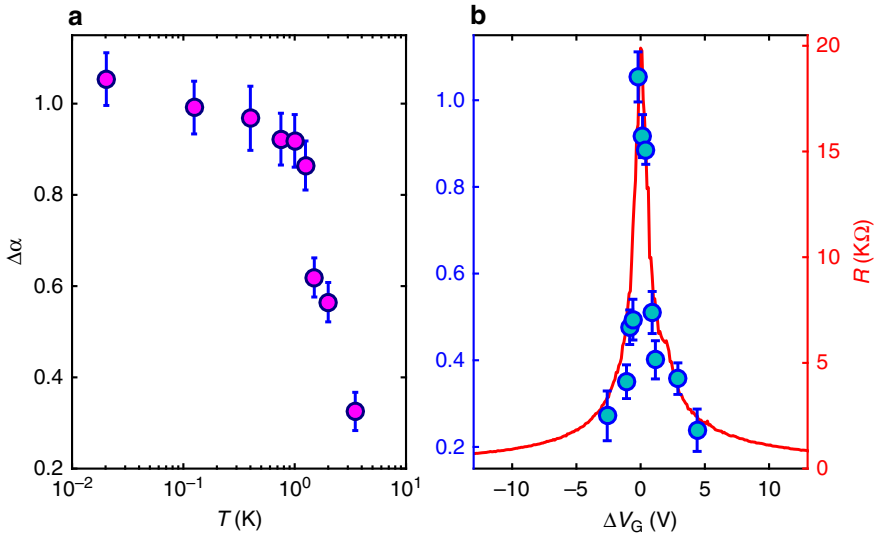

Fig. 5 Width of the multifractal spectrum. **a** Dependence of the width $\Delta\alpha$ on temperature at $\Delta V_G = 0.2$ V; the data were obtained from the UCF plots shown in Fig. 2a. **b** Blue filled circles (left axis) show the dependence of the width of the multifractal spectrum, $\Delta\alpha$ on ΔV_G; the data were obtained at 20 mK. The red line shows the dependence of R on V_G, measured at 20 mK (right axis). It is clear from the plot that $\Delta\alpha$ is large only over a narrow range of gate voltage around $\Delta V_G = 0$ V, and sharply decreases as the system is driven away from the Dirac point. The error bars in **a**, **b** represent the standard deviation in $\Delta\alpha$

high magnetic fields $B_H \simeq \phi_0/A_0$ ($\simeq 10^5$ T for our samples), where $\phi_0 = 2\pi\hbar/e$ is the flux quantum and A_0 is the unit cell area. Our measurements use very low-magnitude magnetic fields (≲0.2 T); this rules out a quasi-periodicity-induced multifractal UCF.

The most compelling explanation of the multifractal UCF we observe in our SLG samples is an incipient Anderson localization near the charge neutrality point. Multifractality of the local amplitudes of critical eigenstates near Anderson localization has been studied, theoretically, in several quantum-condensed matter systems[19,22–24]. The multifractality of the eigenstates near the critical point directly affects the two-particle correlation function through the generalized diffusion coefficient[62,63], which, in turn, affects the local current fluctuations in the system via the Kubo formula. It is not obvious that this must be reflected in the (macroscopic) conductance, or its moments; however, it is plausible that near the critical point, the UCF may inherit multifractal behavior from its counterpart in the eigenfunctions[64]. Indeed, there are several theoretical predictions of multifractality in transport coefficients including conductance jumps near the percolation threshold in random resistor networks[27,28], conductance fluctuations in quantum Hall transitions[29], and the temperature dependence of the peak height of the conductance at the Anderson localization transition[30].

Spectroscopic studies on single-layer on-substrate graphene devices have revealed that the local potential fluctuations in this system are strongest when E_F is close to the Dirac point[7,9]. This leads to electronic states that are quasi-localized[65–67]. Such

quasi-localized states have a high inverse participation ratio[6] that can lead to the multifractality seen in our experiments. If this is true, then the multifractality in the UCF should be largest near the Dirac point; and then fall off on either side of it. In Fig. 5 we show the dependence of $\Delta\alpha$ on T and ΔV_G for the device G28M6 (data obtained for other devices are qualitatively similar). We observe that $\Delta\alpha$ is indeed largest near $\Delta V_G = 0$ and at low T, where the conductance of the device is of the order of e^2/h, and it sharply decreases as either T or the magnitude of ΔV_G increases. Similarly, as T is increased, thermal scattering increases quasiparticle dephasing, and eventually at high T, when $L_\phi \sim L_T \ll L$, quantum-interference effects are masked. From our observation that a large multifractality arises only when quantum interference-induced charge carrier localization is significant, we propose that an incipient Anderson localization near the Dirac point is the most plausible origin of multifractal UCF in SLG.

This interpretation of the multifractality of the UCF in SLG devices is based on previous theoretical predictions and analysis. We summarize our argument below.

Conductance fluctuations, as a function of the magnetic field, have been shown to have a fractional fractal dimensions in some simple, one-dimensional, quantum systems, e.g., the kicked rotor[64,68]. In these systems, such a fractional fractal dimension arises if one of the following conditions holds: (1) The PDF $P(t)$, of the charge carrier survival time t, has a power-law form $P(t) \propto t^{-\gamma}$ at large t (as opposed to an exponential decay); (2) the energy correlation $C(\Delta E)$ of elements of the S-matrix exhibit power laws (i.e., $C(\Delta E) \propto (\Delta E)^{-\gamma}$)[31,34,68,69]. Such survival probabilities are related to the conductance[64,68]; and their multifractal behavior has been explored[25].

At the Anderson localization transition, it is known that both the probability density function describing the diffusion of a wave-packet and the two-particle correlation function decay algebraically with a fractional power[62,63,70]. Hence, as in the case of the simple quantum systems mentioned above, we may expect multifractal fluctuations of the conductance at the Anderson localization transition. However, to the best of our knowledge, there are no exact, analytical results that yield a one-to-one correspondence between the multifractality of a critical wavefunction and the multifractality of the magnetoconductance. Thus, we propose that the multifractality of the critical wavefunctions at the Anderson localization is the most plausible cause of the multifractality of the UCF we have observed.

In conclusion, we have uncovered and quantified the multifractal structure of mesoscopic conductance fluctuations in SLG devices. We speculate that our results are indicative of an incipient Anderson localization in this system. In particular, we quantify the multifractality of transport in a quantum condensed matter system. There may well be multifractality in transport properties in systems other than graphene, and that multifractality is not unique to graphene. Our work provides a natural framework for studying the multifractality of such transport properties.

Methods

Sample fabrication. The graphene flakes were exfoliated from natural graphite onto highly doped Si wafer with thermally grown, 285-nm thick SiO_2 on top. SLG flakes were identified by optical microscopy, and further, confirmed by Raman spectroscopy, or by measurement of integer quantum-hall plateau positions. Electrical contacts to the SLG were made by standard electron-beam lithography followed by thermal evaporation of 5 ~ 7 nm chromium and 60 nm gold. The highly doped Si was used as the back-gate electrode, and the SiO_2 was used as the gate dielectric, which enabled us to tune the charge carrier density, and hence the Fermi level of the device, globally.

Measurement technique. The devices were pumped overnight, before cooling down, to remove moisture and other adsorbents from the graphene surface. The electrical transport characteristics of the devices were measured in a cryogen-free Oxford Instruments Triton 400 dilution refrigerator. Cryogenic filters were used to remove high-frequency noise. The conductance of the device were measured in standard low-frequency ac lock-in measurement technique, in a four-probe configuration. The biasing current (typically 0.25–0.5 nA) was kept sufficiently small to avoid electron heating.

Data analysis. The computation of the fractal dimension of the data were carried out using the Ketzmeric variance method. The multifractal exponents were computed following Multifractal Detrended Fluctuation Analysis method. The details of these methods have been discussed in the Supplementary Note 5 and Supplementary Note 6, respectively.

Data availability. The data that support the plots within this paper and other findings of this study are available from the corresponding author on reasonable request.

Received: 28 September 2017 Accepted: 15 November 2017
Published online: 22 February 2018

References

1. Evers, F. & Mirlin, A. D. Anderson transitions. *Rev. Mod. Phys.* **80**, 1355–1417 (2008).
2. Ludwig, A. W. W., Fisher, M. P. A., Shankar, R. & Grinstein, G. Integer quantum hall transition: an alternative approach and exact results. *Phys. Rev. B* **50**, 7526–7552 (1994).
3. Cheianov, V. V. & Falko, V. I. Selective transmission of dirac electrons and ballistic magnetoresistance of *n-p* junctions in graphene. *Phys. Rev. B* **74**, 041403 (2006).
4. Aleiner, I. L. & Efetov, K. B. Effect of disorder on transport in graphene. *Phys. Rev. Lett.* **97**, 236801 (2006).
5. Katsnelson, M. I., Novoselov, K. S. & Geim, A. K. Chiral tunnelling and the klein paradox in graphene. *Nat. Phys.* **2**, 620–625 (2006).
6. Pereira, V. M., Guinea, F., Lopes dos Santos, J. M. B., Peres, N. M. R. & Castro Neto, A. H. Disorder induced localized states in graphene. *Phys. Rev. Lett.* **96**, 036801 (2006).
7. Samaddar, S., Yudhistira, I., Adam, S., Courtois, H. & Winkelmann, C. B. Charge puddles in graphene near the dirac point. *Phys. Rev. Lett.* **116**, 126804 (2016).
8. Bostwick, A. et al. Quasiparticle transformation during a metal-insulator transition in graphene. *Phys. Rev. Lett.* **103**, 056404 (2009).
9. Jung, S. et al. Evolution of microscopic localization in graphene in a magnetic field from scattering resonances to quantum dots. *Nat. Phys.* **7**, 245–251 (2011).
10. Ponomarenko, L. A. et al. Tunable metal-insulator transition in double-layer graphene heterostructures. *Nat. Phys.* **7**, 958–961 (2011).
11. Mandelbrot, B. B. *The Fractal Geometry of Nature* (Freeman, San Francisco, 1982).
12. Ivanov, P. C.h. et al. Multifractality in human heartbeat dynamics. *Nature* **399**, 461–465 (1999).
13. Lawrence, J. K., Ruzmaikin, A. A. & Cadavid, A. C. Multifractal measure of the solar magnetic field. *Astrophys. J.* **417**, 805 (1993).
14. Oudjemia, S., Girault, J. M., Derguini, N. E. & Haddab, S. in *2013 8th International Workshop on Systems, Signal Processing and their Applications (WoSSPA)* (ed.Boualem Boashash) 244–249 (IEEEXplore, USA, 2013).
15. Frisch, U. *Turbulence: the legacy of AN Kolmogorov* (Cambridge university press, Cambridge, UK, 1995).
16. Benzi, R., Paladin, G., Parisi, G. & Vulpiani, A. On the multifractal nature of fully developed turbulence and chaotic systems. *J. Phys. A Math. Gen.* **17**, 3521 (1984).
17. Castellani, C. & Peliti, L. Multifractal wavefunction at the localisation threshold. *J. Phys. A Math. Gen.* **19**, L429 (1986).
18. Janssen., M. Statistics and scaling in disordered mesoscopic electron systems. *Phys. Rep.* **295**, 1–91 (1998).
19. Mirlin, A. D. Statistics of energy levels and eigenfunctions in disordered systems. *Phys. Rep.* **326**, 259–382 (2000).
20. Grussbach, H. & Schreiber, M. Determination of the mobility edge in the anderson model of localization in three dimensions by multifractal analysis. *Phys. Rev. B* **51**, 663–666 (1995).
21. Burmistrov, I. S., Gornyi, I. V. & Mirlin, A. D. Multifractality and electron-electron interaction at anderson transitions. *Phys. Rev. B* **91**, 085427 (2015).
22. Burmistrov, I. S., Gornyi, I. V. & Mirlin, A. D. Multifractality at anderson transitions with coulomb interaction. *Phys. Rev. Lett.* **111**, 066601 (2013).
23. Gruzberg, I. A., Mirlin, A. D. & Zirnbauer, M. R. Classification and symmetry properties of scaling dimensions at anderson transitions. *Phys. Rev. B* **87**, 125144 (2013).

24. Barrios-Vargas, J. E. & Naumis, G. G. Electron localization in disordered graphene for nanoscale lattice sizes: multifractal properties of the wavefunctions. *2D Mater.* **1**, 011009 (2014).
25. Facchini, A., Wimberger, S. & Tomadin, A. Multifractal fluctuations in the survival probability of an open quantum system. *Phys. A* **376**, 266–274 (2007).
26. Monthus, C. & Garel, T. Statistics of the two-point transmission at anderson localization transitions. *Phys. Rev. B* **79**, 205120 (2009).
27. Rammal, R., Tannous, C., Breton, P. & Tremblay, A. M. S. Flicker (1/*f*) noise in percolation networks: a new hierarchy of exponents. *Phys. Rev. Lett.* **54**, 1718–1721 (1985).
28. Roux, S., Hansen, A. & Hinrichsen, E. L. Multifractality of conductance jumps in percolation. *Phys. Rev. B* **43**, 3601–3612 (1991).
29. Brandes T., Schweitzer, L. & Kramer, B. Multifractal wave functions and inelastic scattering in the integer quantum hall effect. *Phys. Rev. Lett.* **72**, 3582–3585 (1994).
30. Polyakov, D. G. Critical conductance of a mesoscopic system: Interplay of the spectral and eigenfunction correlations at the metal-insulator transition. *Phys. Rev. Lett.* **81**, 4696–4699 (1998).
31. Hegger, H. et al. Fractal conductance fluctuations in gold nanowires. *Phys. Rev. Lett.* **77**, 3885–3888 (1996).
32. Micolich, A. P. et al. Evolution of fractal patterns during a classical-quantum transition. *Phys. Rev. Lett.* **87**, 036802 (2001).
33. Sachrajda, A. S. et al. Fractal conductance fluctuations in a soft-wall stadium and a sinai billiard. *Phys. Rev. Lett.* **80**, 1948–1951 (1998).
34. Ketzmerick, R. Fractal conductance fluctuations in generic chaotic cavities. *Phys. Rev. B* **54**, 10841–10844 (1996).
35. Ujiie, Y., Yumoto, N., Morimoto, T., Aoki, N. & Ochiai, Y. Fractal behaviour in graphene open quantum dot. *J. Phys. Conf. Ser.* **109**, 012035 (2008).
36. Meiss, J. D. & Ott, E. Markov tree model of transport in area-preserving maps. *Phys. D.* **20**, 387–402 (1986).
37. Geisel, T., Zacherl, A. & Radons, G. Generic (1/*f*) noise in chaotic hamiltonian dynamics. *Phys. Rev. Lett.* **59**, 2503–2506 (1987).
38. Novoselov, K. S. A. et al. Two-dimensional gas of massless dirac fermions in graphene. *Nature* **438**, 197–200 (2005).
39. Chen, Y.-F. et al. Magnetoresistance in single-layer graphene: weak localization and universal conductance fluctuation studies. *J. Phys. Condens. Matter* **22**, 205301 (2010).
40. Berger, C. et al. Electronic confinement and coherence in patterned epitaxial graphene. *Science* **312**, 1191–1196 (2006).
41. Bohra, G., Somphonsane, R., Ferry, D. K. & Bird, J. P. Robust mesoscopic fluctuations in disordered graphene. *Appl. Phys. Lett.* **101**, 093110 (2012).
42. Tikhonenko, F. V., Horsell, D. W., Gorbachev, R. V. & Savchenko, A. K. Weak localization in graphene flakes. *Phys. Rev. Lett.* **100**, 056802 (2008).
43. Horsell, D. W. et al. Mesoscopic conductance fluctuations in graphene. *Solid State Commun.* **149**, 1041–1045 (2009).
44. Gorbachev, R. V., Tikhonenko, F. V., Mayorov, A. S., Horsell, D. W. & Savchenko, A. K. Weak localization in bilayer graphene. *Phys. Rev. Lett.* **98**, 176805 (2007).
45. Mohanty, P. & Webb, R. A. High-field measurements of electron decoherence time in metallic nanowires: Switching off magnetic impurity spins. *Phys. Rev. Lett.* **91**, 066604 (2003).
46. Mohanty, P. & Webb, R. A. Decoherence and quantum fluctuations. *Phys. Rev. B* **55**, R13452–R13455 (1997).
47. Pierre, F. et al. Dephasing of electrons in mesoscopic metal wires. *Phys. Rev. B* **68**, 085413 (2003).
48. Liu, B. et al. Conductance fluctuations in graphene in the presence of long-range disorder. *J. Phys. Condens. Matter* **28**, 135302 (2016).
49. Gao-Feng, G. & Wei-Xing, Z. Detrending moving average algorithm for multifractals. *Phys. Rev. E* **82**, 011136 (2010).
50. Wei-Xing, Z. The components of empirical multifractality in financial returns. *Europhys. Lett.* **88**, 28004 (2009).
51. Grassberger, P. & Procaccia, I. Characterization of strange attractors. *Phys. Rev. Lett.* **50**, 346–349 (1983).
52. Kellay, H. & Goldburg, W. I. Two-dimensional turbulence: a review of some recent experiments. *Rep. Progress. Phys.* **65**, 845 (2002).
53. Boffetta, G. & Ecke, R. E. Two-dimensional turbulence. *Annu. Rev. Fluid. Mech.* **44**, 427–451 (2012).
54. Heller, E. J. Bound-state eigenfunctions of classically chaotic hamiltonian systems: Scars of periodic orbits. *Phys. Rev. Lett.* **53**, 1515–1518 (1984).
55. Harper, P. G. The general motion of conduction electrons in a uniform magnetic field, with application to the diamagnetism of metals. *Proc. Phys. Soc. Lond. Sect. A* **68**, 879 (1955).
56. Hofstadter., D. R. Energy levels and wave functions of bloch electrons in rational and irrational magnetic fields. *Phys. Rev. B* **14**, 2239–2249 (1976).
57. Ostlund, S., Pandit, R., Rand, D., Schellnhuber, H. J. & Siggia, E. D. One-dimensional schrödinger equation with an almost periodic potential. *Phys. Rev. Lett.* **50**, 1873–1876 (1983).
58. Sena, S. H. R., Pereira, J. M. Jr, Farias, G. A., Vasconcelos, M. S. & Albuquerque, E. L. Fractal spectrum of charge carriers in quasiperiodic graphene structures. *J. Phys. Condens. Matter* **22**, 465305 (2010).
59. Zurek, W. H. Pointer basis of quantum apparatus: Into what mixture does the wave packet collapse? *Phys. Rev. D.* **24**, 1516–1525 (1981).
60. Huang, L., Lai, Y.-C., Ferry, D. K., Goodnick, S. M. & Akis, R. Relativistic quantum scars. *Phys. Rev. Lett.* **103**, 054101 (2009).
61. Ostlund, S. & Pandit, R. Renormalization-group analysis of the discrete quasiperiodic schrödinger equation. *Phys. Rev. B* **29**, 1394–1414 (1984).
62. Brandes, T., Huckestein, B. & Schweitzer, L. Critical dynamics and multifractal exponents at the anderson transition in 3d disordered systems. *Ann. Phys.* **508**, 633–651 (1996).
63. Brooks Harris, A. & Aharony, A. Anomalous diffusion, superlocalization and hopping conductivity on fractal media. *Europhys. Lett.* **4**, 1355 (1987).
64. Benenti, G., Casati, G., Guarneri, I. & Terraneo, M. Quantum fractal fluctuations. *Phys. Rev. Lett.* **87**, 014101 (2001).
65. Ugeda, M. M., Brihuega, I., Guinea, F. & Gómez-Rodrguez, J. M. Missing atom as a source of carbon magnetism. *Phys. Rev. Lett.* **104**, 096804 (2010).
66. Shytov, A. V., Katsnelson, M. I. & Levitov, L. S. Vacuum polarization and screening of supercritical impurities in graphene. *Phys. Rev. Lett.* **99**, 236801 (2007).
67. Sarma, S. Das, S. A. & Hwang, E. H. and Enrico Rossi. Electronic transport in two-dimensional graphene. *Rev. Mod. Phys.* **83**, 407–470 (2011).
68. Casati, G., Guarneri, I. & Maspero, G. Fractal survival probability fluctuations. *Phys. Rev. Lett.* **84**, 63–66 (2000).
69. Lai, Y.-C., Blümel, R., Ott, E. & Grebogi, C. Quantum manifestations of chaotic scattering. *Phys. Rev. Lett.* **68**, 3491–3494 (1992).
70. Nakayama, T. & Yakubo, K. *Fractal Concepts in Condensed Matter Physics (Springer Series in Solid-State Sciences)* (Springer, Berlin, Heidelberg, 2013).

Acknowledgements

We acknowledge discussions with AD. Mirlin and S. Bhattacharjee. A.B. acknowledges financial support from Nanomission, DST, Govt. of India project SR/NM/NS-35/2012; SERB, DST, Govt. of India and Indo-French Centre for the Promotion of Advanced Recearch (CEFIPRA). K.R.A. thanks CSIR, MHRD, Govt. of India for financial support. S.S.R. acknowledge financial support from the AIRBUS Group Corporate Foundation Chair in Mathematics of Complex Systems established in ICTS-TIFR, the support from DST, Govt. of India, project ECR/2015/000361, and the Indo-French Center for Applied Mathematics (IFCAM). R.P. acknowledges DST, Govt. of India for support. N.P. thanks UGC, Govt. of India for financial support.

Author contributions

K.R.A and A.B. designed the experiment, fabricated the devices and carried out the measurements. K.R.A., A.B., N.P., S.S.R. and R.P. carried out the data analysis. All authors discussed the results and wrote the paper.

Additional information

Supplementary information is available for this paper at https://doi.org/10.1038/s42005-017-0001-4.

Competing interests: The authors declare no competing financial interests.

Reprints and permission information is available online at http://npg.nature.com/reprintsandpermissions/

Publisher's note: Springer Nature remains neutral with regard to jurisdictional claims in published maps and institutional affiliations.